European Journal of Mechanics A/Solids 44 (2014) 91–103

Contents lists available at ScienceDirect

European Journal of Mechanics A/Solids

journal homepage: www.elsevier.com/locate/ejmsol

Legendre spectral element method with nearly incompressible materials

Y.T. Peet [a,b,*], P.F. Fischer [b]

[a] School for Engineering of Matter, Transport and Energy, Arizona State University, Tempe, AZ 85287-6106, USA
[b] Mathematics and Computer Science Division, Argonne National Laboratory, Argonne, IL 60439, USA

ARTICLE INFO

Article history:
Received 21 January 2013
Accepted 8 October 2013
Available online 17 October 2013

Keywords:
Spectral element method
Nearly incompressible materials
Poisson locking

ABSTRACT

We investigate convergence behavior of a spectral element method based on Legendre polynomial shape functions solving linear elasticity equations for a range of Poisson's ratios of a material. We document uniform convergence rates independent of Poisson's ratio for a wide class of problems with both straight and curved elements in two and three dimensions, demonstrating locking-free properties of the spectral element method with nearly incompressible materials. We investigate computational efficiency of the current method without a preconditioner and with a simple mass-matrix preconditioner, however no attempt to optimize a choice of a preconditioner was made.

1. Introduction

Spectral element methods (SEM), which essentially represent a hybrid between finite-element methods (FEM) and spectral methods, have received increased attention during the past two decades because they retain an exponential accuracy of global spectral methods while allowing for a geometrical flexibility of *h*-type FEM. Originally introduced in the field of computational fluid dynamics (Patera, 1984; Fischer and Patera, 1991; Deville et al., 2002), spectral element methods have been adopted for elastostatics (Pavarino and Widlund, 2000a, 2000b) and elastodynamics (Casadei et al., 2002; Stupazzini and Zambelli, 2005; Dong and Yosibash, 2009) problems, modeling of elastic wave propagation in seismology (Komatitsch et al., 1999; Chaljub et al., 2003; Komatitsch et al., 2005), medical diagnostics (Brigham et al., 2011), and damage detection (Ha and Chang, 2010) by high-frequency ultrasound excitation. In addition to forward problems, SEM methods have also been applied to a solution of adjoint problems (Tromp et al., 2008) as those encountered in tomography, inverse acoustics, data assimilation and optimization.

Spectral element methods are similar to *hp* finite-element methods (Szabó and Babuška, 1991) in which grid refinement can be achieved both by increasing the number of elements (*h*-refinement) and by increasing the polynomial order of approximation within each element (*p*-refinement). The advantage of higher-order *p* and *hp* finite-element methods is that they are able to eliminate the phenomenon of locking present with low-order FEM (Vogelius, 1983; Babuška and Suri, 1992a, 1992b; Suri, 1996). Locking is defined as significant deterioration or complete loss of convergence when a certain parameter approaches its limiting value (Babuška and Suri, 1992a, 1992b; Suri, 1996; Hughes, 1987). One important type of locking is volumetric, or Poisson, locking, which occurs when Poisson's ratio ν of an isotropic elastic material approaches 0.5. As this situation occurs, the divergence of a displacement field approaches zero, representing the condition of material incompressibility. Nearly incompressible behavior is peculiar to viscoelastic materials such as rubberlike polymers and elastomers (polyamide, polystyrene, polycarbonate, polyurethane, butadiene, natural rubber, etc.) (Mott et al., 2008). In addition, soft biological tissues such as endothelium, smooth muscle cells, and adventitia forming the blood vessel walls exhibit similar rubberlike behavior (Humphrey, 2003) and are often modeled as elastic incompressible materials (Shim and Kamm, 2002; Figueroa et al., 2006; Valencia and Solis, 2006).

When nearly incompressible materials are modeled with low-order *h*-type finite elements, Poisson locking results in a poor numerical solution that does not improve, or improves very slowly, with grid refinement (Suri, 1996; Gopalakrishnan, 2002). Locking occurs because of the need to satisfy the divergence-free constraint on displacements, one per element, which, in the case of *h*-refinement with low *p*, results in a number of constraints comparable to the number of degrees of freedom (Szabó et al., 1989; Yu

* Corresponding author. School for Engineering of Matter, Transport and Energy, Arizona State University, Tempe, AZ 85287-6106, USA. Tel.: +1 480 965 0735.
E-mail addresses: ypeet@asu.edu, yuliapeet@gmail.com (Y.T. Peet), fischer@mcs.anl.gov (P.F. Fischer).

0997-7538/$ – see front matter © 2013 Elsevier Masson SAS. All rights reserved.
http://dx.doi.org/10.1016/j.euromechsol.2013.10.004

et al., 1993). To remedy the situation, one must reduce the number of constraints per degree of freedom (Nagtegaal et al., 1974). One way to do it is to enforce the constraints in a variational, rather than exact form, as is done with the reduced/selective integration (Malkus and Hughes, 1978), field-consistent approach (Prathap, 1993) and mixed methods, where the divergence constraint is introduced through a Lagrange multiplier (Brezzi and Fortin, 1991). Additionally, in case when the Poisson's ratio is equal to 0.5, a scalar potential (displacement potential) formulation can be used, as in the case of acoustic wave propagation in a fluid media (Cristini and Komatitsch, 2012).

Higher-order p and hp methods present an alternative solution for eliminating locking by satisfying the appropriate constraints exactly; they are able to do so because of the elevated number of degrees of freedom per element and inherently low constraint ratio. It has been shown theoretically (Vogelius, 1983; Babuška and Suri, 1992a; Suri, 1996) and demonstrated numerically (Suri, 1996; Szabó et al., 1989; Heisserer et al., 2008) that in p and hp versions of FEM the error measured in the energy norm converges at the same rate independent of Poisson's ratio. Spectral element methods are closely related to hp finite element methods. They both employ high-order polynomial shape functions to discretize the solution. The important difference is the form of the shape functions: they are constructed from Legendre polynomials and are of hierarchical type for hp finite elements (Szabó and Babuška, 1991; Babuška and Suri, 1994), while they correspond to Lagrange interpolating polynomials defined on Gauss–Lobatto–Legendre points and constitute a nodal basis for spectral element methods (Deville et al., 2002; Pavarino and Widlund, 2000a). This results in different quadrature rules and different structure of a mass matrix: it is full for hp finite-element methods, while it is diagonal for spectral elements. This allows SEM methods to benefit from more efficient inversion and tensor-product factorizations, while hierarchical hp-FEM methods are better suited for adaptive refinement (Sprague and Geers, 2007). Due to a closely-related high-order foundation of both methods, spectral element and hp finite element methods are expected to possess similar locking-free properties associated with the higher-order approximation; however, due to important differences in formulation and numerics, a separate study verifying this fact in a spectral element formulation is needed. In spite of a popularity of spectral element methods, their behavior with nearly incompressible materials in its original (displacement) formulation have not been documented.

Pavarino et al. (Pavarino and Widlund, 2000a, 2000b; Pavarino, 1997; Pavarino et al., 2010) theoretically investigated behavior of several preconditioning schemes for Legendre spectral element discretization of displacement formulation for compressible materials (Pavarino and Widlund, 2000a) and mixed formulation for incompressible materials (Pavarino and Widlund, 2000b; Pavarino, 1997; Pavarino et al., 2010). Sprague et al. (Sprague and Geers, 2007; Brito and Sprague, 2012) documented computational studies of convergence of Legendre spectral element formulation for a 1D Timoshenko beam (Sprague and Geers, 2007) and 2D Reissner-Mindlin plate (Brito and Sprague, 2012) using Poisson's ratio $\nu = 0.3$. Dong and Yosibash (2009) computationally investigated convergence of Jacobi spectral element formulation with 3D elasticity equations, also using $\nu = 0.3$. Few other studies with spectral elements, mostly with application to seismology, considered Earth-like solids with Poisson's ratios of 0.25–0.33 (Stupazzini and Zambelli, 2005; Komatitsch et al., 1999; Chaljub et al., 2003; Komatitsch et al., 2005). The main goal of this paper is to investigate convergence properties of Legendre spectral element formulation for steady linear elasticity problems for a range of Poisson's ratios, from compressible ($\nu = 0.3$) to nearly incompressible (up to $\nu = 0.4999999999$). We also look at the computational efficiency of the method and compare the iteration counts of a conjugate gradient solver with and without a preconditioner with the mixed spectral-element formulation of Pavarino (1997). No attempt at finding a good preconditioner has been made in the current study. This point will be addressed in the future works.

The paper is organized as follows. In Section 2, we present the governing equations and the spectral element discretization. In Section 3, we verify that the discretization scheme passes the inf-sup test. In Section 4, we follow Refs. (Babuška and Suri, 1992a, 1992b; Suri, 1996) to arrive at a computable measure of locking. In Section 5, we use this measure to report the locking properties of the spectral element method in two and three dimensions with straight and curved elements, as well as on highly distorted meshes. In Section 6, we look at the computational efficiency of the current method and compare the iteration counts with mixed spectral-element methods (Pavarino, 1997). In Section 7, we draw conclusions.

2. Problem formulation

In this section, we present the problem formulation, including governing equations and their numerical discretization.

2.1. Equations and the variational form

We consider linear elasticity equations

$$\nabla\cdot\sigma + \mathbf{f} = 0, \tag{1}$$

where σ is the Cauchy stress tensor, and $\mathbf{f}$ is the body force per unit volume. The method proceeds by casting Eq. (1) into an equivalent variational form. Let $\Omega\in R^d$, $d = 2, 3$, be a domain of interest and $\partial\Omega = \partial\Omega_D \cup \partial\Omega_N$ be its boundary decomposed into the parts with Dirichlet and Neumann (traction) boundary conditions. Define the following proper subspaces of the $H^1(\Omega)^d$ Sobolev space (space of vector-valued functions square-integrable over Ω whose derivatives are also square-integrable over Ω):

$$\begin{aligned}\mathbf{X} &= \left\{\mathbf{v}(\mathbf{x})\in H^1(\Omega)^d : \mathbf{v}(\mathbf{x})\big|_{\partial\Omega_D} = \mathbf{u}_D(\mathbf{x})\right\},\\ \mathbf{X}_0 &= \left\{\mathbf{v}(\mathbf{x})\in H^1(\Omega)^d : \mathbf{v}(\mathbf{x})\big|_{\partial\Omega_D} = 0\right\}.\end{aligned} \tag{2}$$

The variational formulation of the linear elasticity problem is as follows: Find the displacement field $u(\mathbf{x})\in\mathbf{X}$ such that $\forall\ \mathbf{v}(\mathbf{x})\in\mathbf{X}_0$

$$-\int_\Omega \sigma(\mathbf{u}) : \varepsilon(\mathbf{v})\mathrm{d}\Omega + \int_{\partial\Omega_N} \mathbf{t}\cdot\mathbf{v}\mathrm{d}\Gamma + \int_\Omega \mathbf{f}\cdot\mathbf{v}\mathrm{d}\Omega = 0. \tag{3}$$

Here $\mathbf{t}$ is the external traction force applied on $\partial\Omega_N$, and $\varepsilon(\mathbf{v}) = \frac{1}{2}[\nabla\mathbf{v} + (\nabla\mathbf{v})^T]$ is the linearized strain tensor. The vector and tensor inner products are defined as

$$\mathbf{u}\cdot\mathbf{v} = \sum_{i=1}^{d} u_i v_i, \tag{4}$$

$$\sigma(\mathbf{u}) : \varepsilon(\mathbf{v}) = \sum_{i=1}^{d}\sum_{j=1}^{d} \sigma_{ij}(\mathbf{u})\varepsilon_{ij}(\mathbf{v}). \tag{5}$$

For linear elasticity, constitutive equations arise from Hooke's law,

$$\sigma = 2\mu\varepsilon + \lambda\mathrm{tr}(\varepsilon)\mathbf{I}, \tag{6}$$

where

$$\mu = \frac{E}{2(1+\nu)}, \tag{7}$$

$$\lambda = \frac{E\nu}{(1+\nu)(1-2\nu)} \tag{8}$$

for 3D isotropic materials and 2D plane strain formulation, and

$$\lambda = \frac{E\nu}{(1+\nu)(1-\nu)} \tag{9}$$

for 2D plane stress formulation, E is Young's modulus, ν is Poisson's ratio, tr() denotes the trace, and $\mathbf{I}$ is the identity matrix. Introducing constitutive relations (6) into Eq. (5) leads to

$$\sigma(\mathbf{u}) : \varepsilon(\mathbf{v}) = 2\mu(\varepsilon(\mathbf{u}) : \varepsilon(\mathbf{v})) + \lambda \mathrm{div}\mathbf{u}\, \mathrm{div}\mathbf{v}. \tag{10}$$

We denote

$$B_\nu(\mathbf{u},\mathbf{v}) = \int_\Omega [2\mu(\varepsilon(\mathbf{u}) : \varepsilon(\mathbf{v})) + \lambda \mathrm{div}\mathbf{u}\, \mathrm{div}\mathbf{v}]\mathrm{d}\Omega \tag{11}$$

as the bilinear form of linear elasticity.

2.2. Spectral element discretization

In the spectral element method, the computational domain Ω is decomposed into a set of nonoverlapping subdomains (elements) $\Omega = \cup_{e=1}^{\varepsilon}\Omega^e$. In the current method, we assume that for each Ω^e there exists an affine transformation $\widehat{\Omega} = \phi^e(\Omega^e)$ into the reference element $\widehat{\Omega} = [-1,1]^d$, implying that Ω^e are hexahedral. Other choices (prismatic, tetrahedral, etc.) are available (Dong and Yosibash, 2009; Karniadakis and Sherwin2nd ed., 2005), but they will not be pursued here. On the reference element $\widehat{\Omega}$ we introduce $Q_p(\widehat{\Omega})$, the space of polynomial functions of degree p in each spatial variable, and restrict the trial and test functions $\mathbf{u}$ and $\mathbf{v}$ in each element Ω^e to the finite-dimensional spaces $\mathbf{X}^p$ and $\mathbf{X}_0^p$,

$$\begin{aligned}\mathbf{X}^p &= \left\{\mathbf{v}(\mathbf{x})\in\mathbf{X} : v_i\Big|\Omega^e = \psi\circ\phi^e, \psi\in Q_p\left(\widehat{\Omega}\right), i = 1,\ldots d\right\},\\ \mathbf{X}_0^p &= \left\{\mathbf{v}(\mathbf{x})\in\mathbf{X}_0 : v_i\Big|\Omega^e = \psi\circ\phi^e, \psi\in Q_p\left(\widehat{\Omega}\right), i = 1,\ldots d\right\},\end{aligned} \tag{12}$$

where $f\circ g$ denotes a function composition. The basis functions for the polynomial space $Q_p(\widehat{\Omega})$ are chosen to be the tensor product of one-dimensional Lagrange interpolating polynomials $h_i(r)$, $r\in[-1,1]$, on the Gauss–Lobatto–Legendre (GLL) quadrature points $\xi_m\in[-1,1]$, $i,m = 0,\ldots,p$, satisfying $h_i(\xi_m) = \delta_{im}$. Every function in $Q_p(\widehat{\Omega})$ is represented as a tensor product

$$f(\mathbf{x})\Big|_{\widehat{\Omega}} = \sum_{i=0}^{p}\sum_{j=0}^{p}\left\{\sum_{k=0}^{p} f^e_{ij\{k\}} h_i(r)h_j(r)\{h_k(r)\}\right\}, \tag{13}$$

where $f^e_{ij\{k\}}$ are unknown expansion coefficients, and curly brackets contain the extra terms that arise in three dimensions. Derivatives of a function in $Q_p(\widehat{\Omega})$ can be defined analogously through the derivatives of the corresponding Lagrange polynomials:

$$\frac{\partial f}{\partial x_1}(\mathbf{x})\Big|_{\widehat{\Omega}} = \sum_{i=0}^{p}\sum_{j=0}^{p}\left\{\sum_{k=0}^{p} f^e_{ij\{k\}} h_i'(r)h_j(r)\{h_k(r)\}\right\}. \tag{14}$$

The current choice of basis functions allows for an efficient quadrature implementation. In addition, it is continuous across subdomain interfaces (Fischer, 1997). The quadrature rules are defined as

$$\int_{\widehat{\Omega}} f\, g\mathrm{d}\widehat{\Omega} = \sum_{i=0}^{p}\sum_{j=0}^{p}\left\{\sum_{k=0}^{p}\right\} f^e_{ij\{k\}} g^e_{ij\{k\}} \sigma_i\sigma_j\{\sigma_k\} \tag{15}$$

and

$$\int_{\Omega} f\, g\mathrm{d}\Omega = \sum_{e=1}^{\varepsilon}\sum_{i,j,\{k\}=0}^{p} (f\circ\phi^e)_{ij\{k\}}(g\circ\phi^e)_{ij\{k\}}|J^e|_{ij\{k\}}\sigma_i\sigma_j\{\sigma_k\}, \tag{16}$$

where σ_i is the GLL quadrature weight associated with ξ_i and $|J^e|_{ij\{k\}}$ is the Jacobian of the transformation ϕ^e at the point $(\xi_i,\xi_j,\{\xi_k\})$. Thus, for an inner product $\int_\Omega \mathbf{u}\cdot\mathbf{v}\mathrm{d}\Omega$ we can write

$$\int_\Omega \mathbf{u}\cdot\mathbf{v}\mathrm{d}\Omega = \underline{\mathbf{v}}^T\mathbf{B}\underline{u}, \tag{17}$$

where $\underline{\mathbf{u}}, \underline{\mathbf{v}}$ are the vectors with dimensions $\mathcal{N} = \mathrm{d}N, N = \varepsilon(p+1)^d$, of the corresponding expansion coefficients $u^e_{ij\{k\}m}$, $v^e_{ij\{k\}m}$, $i,j,\{k\} = 0,\ldots,p, m = 1,\ldots,d, e = 1,\ldots,\varepsilon$, and $\mathbf{B}$ is the (diagonal) mass matrix. Quadrature for the surface integral $\int_{\partial\Omega_N}\mathbf{t}\cdot\mathbf{v}d\Gamma$ is defined similar to Eq. (16) using summation over the surface nodes on $\partial\Omega_N$ with the corresponding surface quadrature weights and surface Jacobians in place of the volumetric ones. Using the definition of Eq. (14) for derivatives, one can analogously define discrete quadrature for a bilinear form of linear elasticity $B_\nu(\mathbf{u},\mathbf{v})$ of Eq. (11), resulting in a symmetric, positive-definite stiffness matrix $\mathbf{A}$. Although the stiffness matrix is no longer diagonal, the corresponding matrix-vector products can be efficiently evaluated in $O(p^{d+1})$ operations if one retains the matrix tensor-product form in favor of its explicit formation (Orszag, 1980). Applying the corresponding numerical quadrature rules to every integral in the Eq. (3), one can reformulate the original variational problem in discrete form: Find $\underline{\mathbf{U}}\in\mathcal{U}_0^{\mathcal{N}}$ such that $\forall\underline{\mathbf{v}}\in\mathcal{U}_0^{\mathcal{N}}$

$$\underline{\mathbf{v}}^T\mathcal{M}\mathbf{A}\mathcal{M}\underline{\mathbf{U}} = \underline{\mathbf{v}}^T\mathcal{M}\left(\mathbf{B}\underline{f} + \mathbf{B}_N\underline{\mathbf{t}} - \mathbf{A}\mathcal{M}\underline{\mathbf{u}}_D\right), \tag{18}$$

where an additional mask matrix $\mathcal{M}$ is introduced to account for Dirichlet boundary conditions, $\mathbf{v}(\mathbf{x})|_{\partial\Omega_D} = \mathbf{u}_D(\mathbf{x})$; $\mathcal{M}$ is the diagonal matrix having zeros at the nodes corresponding to $\partial\Omega_D$ and ones everywhere else; $\mathcal{U}_0^{\mathcal{N}}$ is the subspace of the vector space $R^{\mathcal{N}}$ enforcing homogeneous Dirichlet boundary conditions. The term $\mathbf{B}_N\underline{\mathbf{t}}$ in the right-hand side accounts for the surface integral $\int_{\partial\Omega_N}\mathbf{t}\cdot\mathbf{v}\mathrm{d}\Gamma$ arising from the traction boundary conditions, where $\mathbf{B}_N$ is obtained from the mass matrix $\mathbf{B}$ by zeroing out all the entries except the entries corresponding to the nodes of $\partial\Omega_N$. This discrete variational problem is equivalent to solving the linear system of equations for the vector $\underline{\mathbf{U}}\in\mathcal{U}_0^{\mathcal{N}}$,

$$\mathbf{K}\underline{\mathbf{U}} = \underline{\mathbf{F}}, \tag{19}$$

where $\mathbf{K} = \mathcal{M}\mathbf{A}\mathcal{M}$ is the global stiffness matrix and the right-hand side $\underline{\mathbf{F}} = \mathcal{M}(\mathbf{B}\underline{f} + \mathbf{B}_N\underline{\mathbf{t}} - \mathbf{A}\mathcal{M}\underline{\mathbf{u}}_D)$. Since the matrix $\mathbf{K}$ is symmetric positive-definite (SPD), classical Conjugate Gradient approach, which is one of the most efficient iterative techniques for solving SPD linear systems (Saad, 2003), is applied to solve the matrix Equation (19). Note that, for example, with the mixed formulation of linear elasticity, a corresponding saddle-point problem results in a symmetric indefinite or even non-symmetric (depending on a preconditioner) system which prohibits the use of the classical

Conjugate Gradient method and calls for more sophisticated approaches, such as CR (Conjugate Residual), Bi-CGStab (Biconjugate Gradient Stabilized) or GMRES (Generalized Minimum Residual) (Pavarino, 1997).

The composite solution satisfying inhomogeneous Dirichlet boundary conditions is obtained as

$$\underline{\mathbf{u}} = \underline{\mathbf{U}} + \underline{\mathbf{u}}_D. \tag{20}$$

3. Inf-sup test

We first show that the displacement-based spectral-element discretization scheme satisfies the inf-sup condition of Brezzi and Babuška (Brezzi and Fortin, 1991)

$$\inf_{q\in L^2(\Omega)} \sup_{\mathbf{v}\in\mathbf{X}_0} \frac{\int_\Omega q(\nabla\cdot\mathbf{v})\mathrm{d}\Omega}{||q||_{L^2}||\mathbf{v}||_{H^1}} \geq \delta > 0. \tag{21}$$

Inf-sup condition (21) is the condition of optimal convergence and, when satisfied, guarantees the absence of locking (Chapelle and Bathe, 1993). For mixed formulation, analytical proof of the inf-sup condition is available for Stokes problem for spectral-element formulation (Maday et al., 1992) and for elasticity problem for more general discrete mixed spaces (Suri and Stenberg, 1996). For displacement formulation, to the authors' knowledge, analytical results are not available.

In spite of the absence of an analytical proof, a convenient numerical test of the inf-sup condition can be applied (Chapelle and Bathe, 1993; Bathe, 1996; Jensen and Vogelius, 1990). We follow the approach of Chapelle and Bathe (1993) who write a discrete form of the inf-sup condition (21) for a displacement method as

$$\inf_{\underline{\mathbf{W}}\in\mathcal{U}_0^N} \sup_{\underline{\mathbf{U}}\in\mathcal{U}_0^N} \frac{\underline{\mathbf{W}}^T\mathbf{G}\underline{\mathbf{U}}}{\sqrt{\underline{\mathbf{W}}^T\mathbf{G}\underline{\mathbf{W}}}\sqrt{\underline{\mathbf{U}}^T\mathbf{S}\underline{\mathbf{U}}}} \geq \delta > 0, \tag{22}$$

where the vectors $\underline{\mathbf{W}}\in\mathcal{U}_0^N$ are discrete representations of the functions $\mathbf{w}(\mathbf{x}) \in \mathbf{X}_0$ whose divergence equals to $q(\mathbf{x})\in L_2(\Omega)$; see (Bathe, 1996) for the details of constructing the matrices **G** and **S**. Numerical test follows by evaluating the inf-sup constant

$$\delta_N = \inf_{\underline{\mathbf{W}}\in\mathcal{U}_0^N} \sup_{\underline{\mathbf{U}}\in\mathcal{U}_0^N} \frac{\underline{\mathbf{W}}^T\mathbf{G}\underline{\mathbf{U}}}{\sqrt{\underline{\mathbf{W}}^T\mathbf{G}\underline{\mathbf{W}}}\sqrt{\underline{\mathbf{U}}^T\mathbf{S}\underline{\mathbf{U}}}} \tag{23}$$

on a sequence of successively-refined meshes (Chapelle and Bathe, 1993). This numerical evaluation is possible due to the result proven in (Brezzi and Fortin, 1991) stating that the inf-sup constant δ_N in Eq. (23) equals to the square-root of the first non-zero eigenvalue λ_1 of the generalized eigenvalue problem $\mathbf{G}\underline{\mathbf{U}} = \lambda\mathbf{S}\underline{\mathbf{U}}$, $\delta_N = \sqrt{\lambda_1}$. We have tested two element shapes: a straight element and a curved element where we have varied the curvature by changing the amplitude of the curved side a, see Fig. 1. The results of the numerical inf-sup test for different values of amplitude a are shown in Fig. 2. Following Chapelle and Bathe (Chapelle and Bathe, 1993), we plot results in the form $\log(\delta_N) = f(\log(1/p))$, where δ_N is the calculated value of the inf-sup expression, and p is the polynomial order. In order to pass the inf-sup test, the inf-sup constant must stay bounded away from zero as the mesh is refined. It is seen that the straight element and curved elements with relatively large amplitudes of up to $a < 15$ pass the inf-sup test. When the amplitude reaches the values of $a \geq 15$ representing high to extreme levels of distortion, the element starts failing at large polynomials orders.

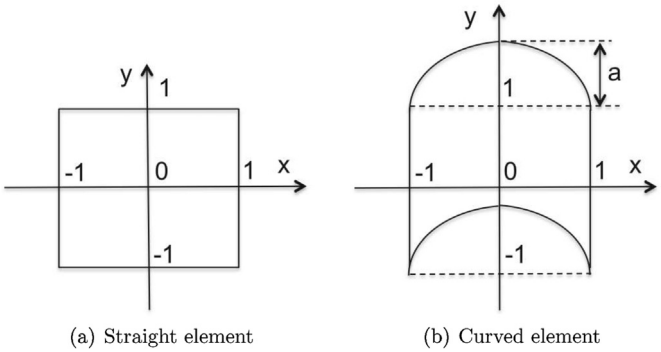

(a) Straight element (b) Curved element

Fig. 1. Element shape for inf-sup test.

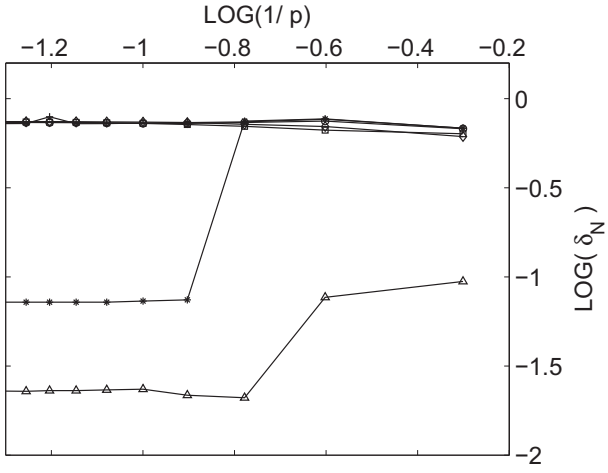

Fig. 2. Inf-sup results. Diamonds, straight element; squares, curved element with amplitude $a = 1$; circles, curved element with amplitude $a = 5$; pluses, curved element with amplitude $a = 10$; stars, curved element with amplitude $a = 15$; triangles, curved element with amplitude $a = 50$.

4. Measure of locking

In this section, we follow Refs. (Babuška and Suri, 1992a, 1992b; Suri, 1996) to define a computable measure of locking.

Let us first introduce several relevant concepts.

- *Solution space* H_ν is the set of exact solutions of Eq. (3).
- *Error functional* $E_\nu(\mathbf{u})$ is the considered error measure.
- *Extension procedure* $\mathcal{F}$ is the rule defining how the space dimension N is to be increased.
- *Parameter set* S is the range of the values of the parameter. In our case, the parameter is the Poisson's ratio ν and the parameter set is $S = [0,0.5)$.

For the extension procedure $\mathcal{F}$, one can define the asymptotic rate of best approximation $F_0(N)$ of functions in $\mathbf{X}_0$ by functions in $\mathbf{X}_0^p$ as

$$F_0(N) = \sup_{\mathbf{w}\in\mathbf{X}_0} \inf_{\mathbf{v}\in\mathbf{X}_0^p} \|\mathbf{w}-\mathbf{v}\|_{H^1}.$$

One would expect $F_0(N)\to 0$ as $N\to\infty$ for the viable methods. According to (Babuška and Suri, 1992a), a procedure $\mathcal{F}$ is called *free from locking*, with respect to the solution sets H_ν, and error measures E_ν, if the following property holds uniformly for all $0 \leq \nu \leq \nu_0$, with $0 < \nu_0 < 0.5$,

$$C_1(\nu_0)F_0(N) \le \sup_{\mathbf{u}_\nu \in H_\nu} E_\nu(\mathbf{u}_\nu - \mathbf{u}_\nu^N) \le C_2(\nu_0)F_0(N), \tag{24}$$

where $C_1(\nu_0)$, $C_2(\nu_0)$ are independent of ν and N.

Related to the concept of locking is the concept of robustness. The extension procedure $\mathcal{F}$ is called *robust* with respect to the solution sets H_ν, and error measures E_ν, $\nu \in S$, if and only if

$$\lim_{N\to\infty} \sup_{\nu} \sup_{\mathbf{u}_\nu \in H_\nu} E_\nu(\mathbf{u}_\nu - \mathbf{u}_\nu^N) = 0.$$

It is called *robust with uniform order* $g(N)$ if and only if

$$\lim_{N\to\infty} \sup_{\nu} \sup_{\mathbf{u}_\nu \in H_\nu} E_\nu(\mathbf{u}_\nu - \mathbf{u}_\nu^N) \le g(N),$$

where $g(N) \to 0$ as $N \to \infty$.

The following theorem leads to a characterization of locking in therms of the *loss in the asymptotic rate of convergence* (Babuška and Suri, 1992a, 1992b; Suri, 1996).

Theorem 1. *$\mathcal{F}$ is free from locking if and only if it is robust with uniform order $F_0(N)$. Moreover, let $f(N)$ be such that*

$$f(N)F_0(N) = g(N) \to \infty \text{ as } N \to \infty.$$

Then, $\mathcal{F}$ shows locking of order $f(N)$ if and only if it is robust with uniform order $g(N)$.

Based on the above theorem, we are going to judge about the locking properties of the spectral element extension procedure $\mathcal{F}$ described above by looking at the order of robustness $g(N)$. For this, the corresponding value of the error measure $E_\nu(\mathbf{u}_\nu - \mathbf{u}_\nu^N)$ for different test cases is calculated, and its limit, $\lim_{N\to\infty} \sup_{\nu} \sup_{\mathbf{u}_\nu \in H_\nu} E_\nu(\mathbf{u}_\nu - \mathbf{u}_\nu^N)$, is compared to the asymptotic rate of best approximation $F_0(N)$, which, for the spectral-element discretization is (Deville et al., 2002; Szabó and Babuška, 1991)

$$F_0(N) = O\left(h^{N^{1/d}}\right) \tag{25}$$

with the constant $h < 1$.

In the current study, we define the error functional $E_\nu(\mathbf{u})$ to be the error in the energy norm (Babuška and Suri, 1992a; Suri, 1996; Szabó et al., 1989; Heisserer et al., 2008; Chilton and Suri, 1997; Yosibash, 1996)

$$E_\nu(\mathbf{u}) = (B_\nu(\mathbf{u},\mathbf{u}))^{1/2}, \tag{26}$$

where $B_\nu(\mathbf{u},\mathbf{u})$ is the bilinear form of linear elasticity defined by Eq. (11).

5. Numerical results

In this section, we use the definition of locking given in the previous section to demonstrate locking and convergence properties of the displacement-based spectral element method on several test cases.

5.1. Straight elements: bending of a beam (plane stress)

In the first test problem, we consider a bending of a narrow cantilever beam of rectangular cross-section under the end load. For this configuration, *plane stress* conditions can be assumed, reducing the problem to a two-dimensional case with Lamé coefficients given by Eqs. (7) and (9). An exact solution to this problem exists (Wang, 1953) and is given in Appendix A.1. We use length $L = 10$, width $d = 1$, Young's modulus $E = 10{,}000$, and end load $P = -3IE/L^3$ (I is the cross-sectional moment of inertia) giving the end beam deflection $v = -1$. The boundary conditions are stress-free at the upper and lower edges, with parabolic shear stress distribution $\tau_{xy} = -P(d^2/4 - y^2)/(2I)$ at the left edge ($x = 0$) and displacements (or Dirichlet) boundary conditions at the right edge ($x = L$). The computational domain consists of $\varepsilon = 5$ rectangular elements. The bent beam and the deflection of the beam centerline compared with the exact solution are shown in Fig. 3 for $\nu = 0.3$, p=4. The agreement is excellent. To quantify the error with p-refinement, we plot the $L_2(\mathbf{u})$ error versus the polynomial order in Fig. 4 for the values of $\nu = 0.3$ and $\nu = 0.5$.

Since the analytical solution is the polynomial of degree 3, the SEM recovers it with machine accuracy for $p = 3$ and higher. Note that for plane stress elasticity, the incompressibility condition $\nu = 0.5$ does not make the governing equations singular because it is $1 - \nu$, and not $1 - 2\nu$ that appears in the denominator of λ (cf. Eqs. (8) and (9)). That explains why the solution is recovered exactly for $\nu = 0.5$ as well as for $\nu = 0.3$ (Fig. 4). Thus, plane stress loading does not represent a challenging test for Poisson locking and will not be considered further.

5.2. Straight elements: unit square (plane strain)

To consider a more challenging test for Poisson locking, we look at a two-dimensional *plane strain* problem, with μ and λ defined by Eqs. (7) and (8). We consider a deformation of a unit square $[0,1] \times [0,1]$, with an exact solution for displacements listed in Appendix A.2. We choose the values $A = (1 - \nu)/a$, $B = -\nu/b$. This choice corresponds to the most general but realistic loading with nonzero divergence

$$\mathrm{div}\mathbf{u} = (1 - 2\nu)\cos(ax)\cos(by),$$

which reduces to zero in the incompressible case $\nu = 0.5$; and with nonzero shear

$$\gamma_{xy} = -[(1 - \nu)b/a - \nu a/b]\sin(ax)\sin(by).$$

We set $a = \pi/2$, $b = \pi/3$, $E = 1000$, and we decompose the domain into four square elements of size 0.5×0.5.

To document the locking properties according to the definition presented in Section 4, we plot the percentage relative error in the energy norm versus $N^{1/d}$ in Fig. 5 for traction and displacement boundary conditions. The plot of relative errors shows that the procedure is robust with the order $F_0(N) = O(h^{N^{1/d}})$, since all the error curves are parallel to the asymptotic rate of best approximation $F_0(N) = h^{N^{1/d}}$ ($h = 0.15$), which, by Theorem 1, confirms the locking-free behavior of the current method.

Results of Fig. 5 correspond well to the results obtained with the p-version FEM (Szabó et al., 1989). The results of (Szabó et al., 1989) indicate that the rate of convergence for $\nu \in [0,0.5)$ is exponential with the relative error proportional to $C(\nu)h^{N^{1/d}}$, where the rate of convergence h does not depend on ν, but the multiplication

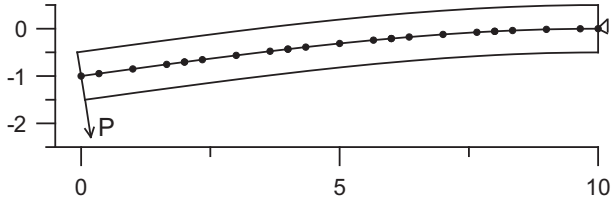

Fig. 3. Bent beam and deflection of the centerline compared with the exact solution (symbols).

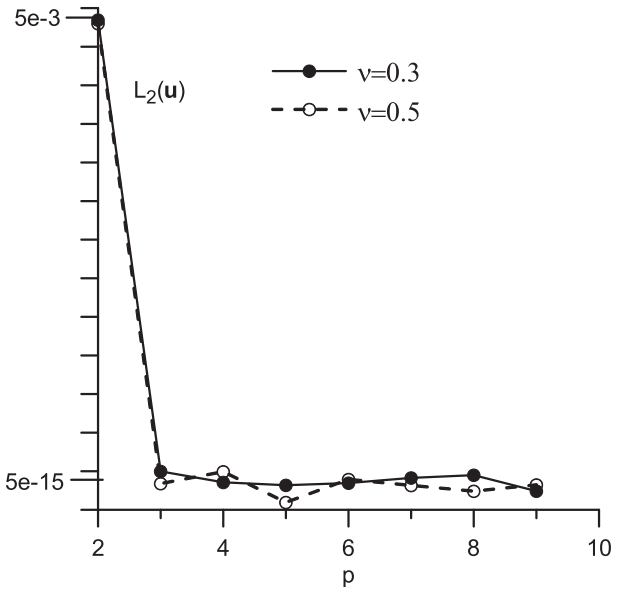

Fig. 4. $L_2(\mathbf{u})$ error versus the polynomial order for a narrow beam in plane stress.

constant C does, which results in convergence curves being parallel but shifted upwards as $\nu \to 0.5$. They also noted the existence of the bounding envelope shown schematically in Fig. 5(a) and (b), representing the error bound when $\nu \to 0.5$, which decreases with N at the rate of $F_0(N)$. Another result is the existence of p_{crit}, the polynomial order for which convergence starts as $\nu \to 0.5$. The value of p_{crit} depends on various factors, such as whether the elements are curved; whether they are triangles or quadrilaterals etc. (p_{crit} is smaller for triangles than for quadrilaterals).

5.3. Straight elements: unit cube

To document the spatial convergence in the full 3D case, we consider the deformation of a unit cube $[0,1] \times [0,1] \times [0,1]$, with an exact solution given in Appendix A.3. With $A = (1-\nu)/a$, $B = -0.5\nu/b$, $C = -0.5\nu/c$, we again recover a general loading situation with nonzero divergence,

$$\operatorname{div} \mathbf{u} = (1-2\nu)\cos(ax)\cos(by)\cos(cz),$$

approaching zero at $\nu \to 0.5$, and nonzero shear strain components γ_{xy}, γ_{xz}, γ_{yz}. We set $a = \pi/2$, $b = \pi/3$, $c = \pi/4$, $E = 1000$ and decompose the domain into eight cubic elements $0.5 \times 0.5 \times 0.5$. Note that most of the previous studies on locking with *hp*-FEM were confined to two dimensions and did not consider three-dimensional cases (Suri, 1996; Szabó et al., 1989; Chilton and Suri, 1997; Yosibash, 1996). Convergence in the energy norm versus $N^{1/d}$ is plotted in Fig. 6 for traction and displacement boundary conditions. The results are almost identical to those of a unit square, showing that the problem dimension by itself does not influence the convergence and locking properties of the spectral element method, at least for straight elements.

5.4. Curved elements: hollow cylinder under internal pressure (plane strain)

To investigate the influence of curved elements on the method's spatial convergence, we look at the problems in cylindrical and spherical configurations. We first consider a long, thick-walled, hollow cylinder under internal pressure resulting in a *plane strain* loading, with an exact solution given, for example, in (Gao, 2003) and documented in Appendix A.4. We set $E = 1000$, internal pressure $P = 100$, the inner and outer radius of the cylinder $r_i = 0.5$ and $r_o = 1$. Because of the plane strain loading, this problem can be considered in 2D. The computational domain consists of a hollow disk with six circumferential elements of the radial width $\Delta r = 0.5$. The computational domain and solution (radial displacement for $\nu = 0.3$) are shown in Fig. 7(a). Note that in order to achieve expected exponential convergence rates for the hollow cylinder, boundary grid nodes and GLL points need to be located precisely on the surface of the cylinder (within the machine accuracy of the numerical computation) in the undeformed configuration. This is required to make sure that boundary conditions are imposed at the correct locations to ensure convergence of the numerical solution to the exact solution, which otherwise would be deteriorated by the numerical errors coming from the boundaries. The required placement of GLL points onto the surface of the cylinder within the machine precision can be ensured by shifting them along the radii to conform to the surface after the elements are initially populated with the GLL points by the automatic mesh partitioning tools in the

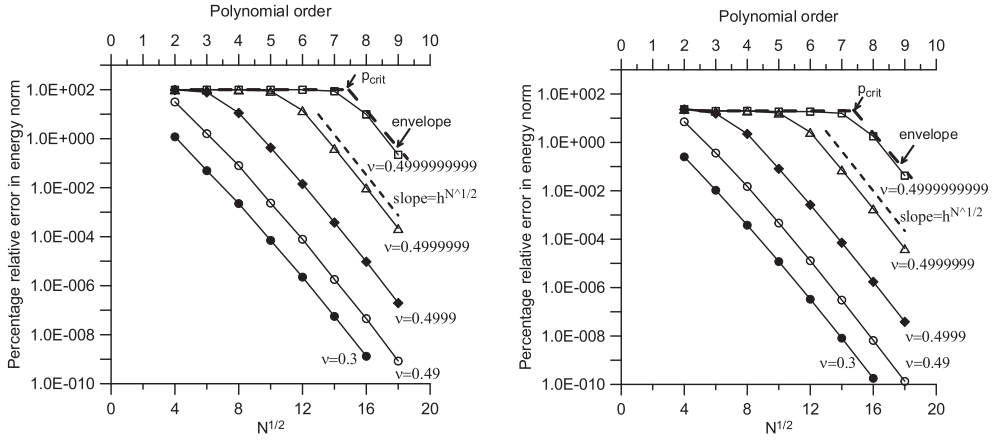

(a) Traction boundary conditions (b) Displacement boundary conditions

Fig. 5. Locking properties for the unit square: error in the energy norm. Dashed line represents the asymptotic curve $h^{N^{1/2}}$, $h = 0.15$.

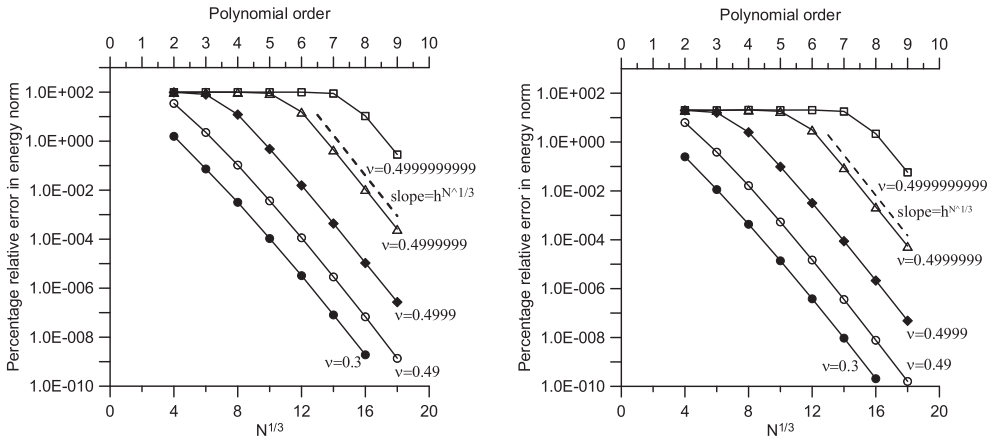

(a) Traction boundary conditions (b) Displacement boundary conditions

Fig. 6. Locking properties for the unit cube: error in the energy norm. Dashed line represents the asymptotic curve $h^{N^{1/3}}$, $h = 0.15$.

code. Note that Suri (1996) also used a special blending technique for the boundary segments to ensure convergence to the exact solution on a segment of an annulus.

Convergence in the energy norm versus $N^{1/d}$ is shown in Fig. 8 for traction and displacement boundary conditions. In the previous studies with *hp* finite-element methods, a decrease in accuracy has been observed for curved elements as compared to straight elements when $\nu \to 0.5$ (Suri, 1996; Chilton and Suri, 1997) due to the fact that it is harder for the trial functions (which under general mappings may no longer be polynomials) to satisfy the incompressibility constraint (Suri, 1996). The effect seemed to be more severe for an *h* version than for a *p* version; for the latter the main deterioration could be summarized as a shift in convergence curves from Cp^{-k} to $C(p-\alpha)^{-k}$ when ν is close to 0.5, where C, k and α are some constants, α depended on the nature of the curved side (Babuška and Suri, 1990). With a spectral-element formulation, increase in error with curved elements has also been observed in various problems (Deville et al., 2002; Schneidesch and Deville, 1993), due to the fact that the quadrature evaluation in the presence of Jacobian matrices of a general mapping is no longer exact. However, despite the increase in errors, an exponential convergence with p was still attained with the SEM in the presence of curvilinear meshes (Schneidesch and Deville, 1993). In our tests with the spectral-element method with curved elements for linear elasticity, we reached similar conclusions. The value of a slope in the exponential rate of convergence $O(h^{N^{1/d}})$ is increased from $h = 0.15$ for straight elements to $h = 0.5$ for the hollow cylinder, which indicates an overall increase in error with curved elements while retaining exponential convergence, consistent with the observations of Schneidesch and Deville (1993). In addition, the value of p_{crit}, the polynomial order for which convergence starts as $\nu \to 0.5$, is increased compared to straight elements, consistent with the shift in convergence curves from Cp^{-k} to $C(p-\alpha)^{-k}$ when $\nu \to 0.5$ observed by Babuška and Suri (1990) with *p*-FEM. Both

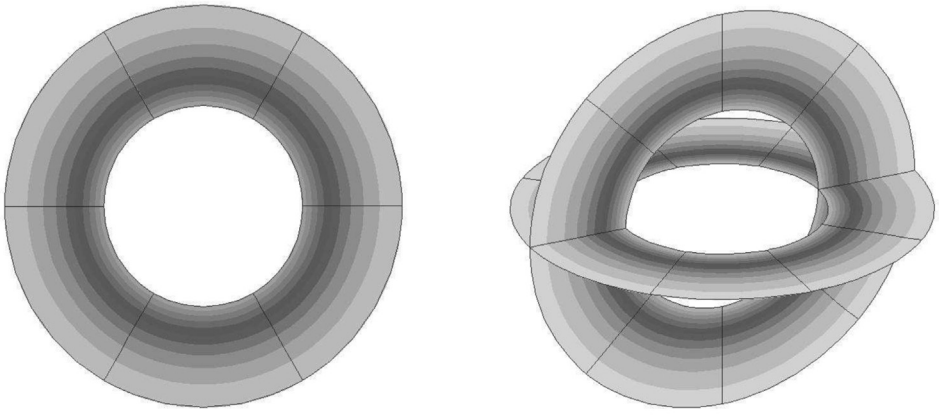

(a) Hollow cylinder. Min displacement 0.05 (at r_0); max displacement 0.1 (at r_i).

(b) Hollow sphere. Min displacement 0.01 (at r_0); max displacement 0.04 (at r_i).

Fig. 7. Meshes with curved elements. Radial displacement u_r is shown.

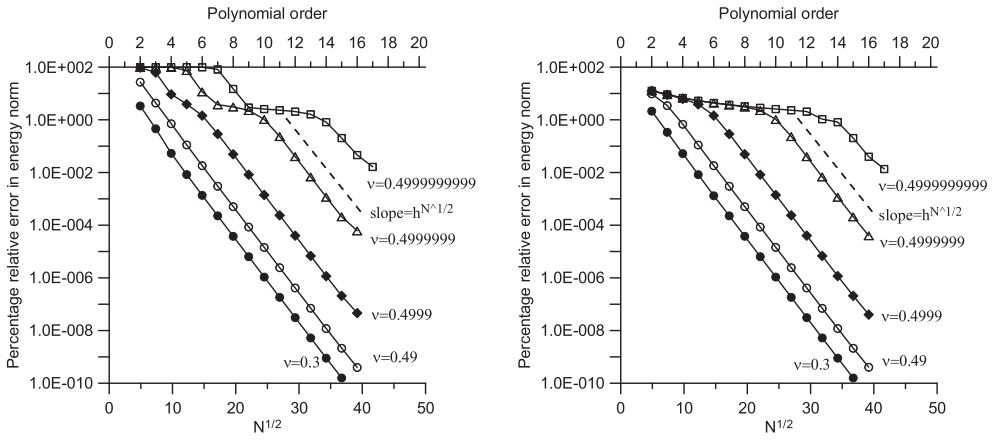

(a) Traction boundary conditions (b) Displacement boundary conditions

Fig. 8. Locking properties for the hollow cylinder: error in the energy norm. Dashed line represents the asymptotic curve $h^{N^{1/2}}$, $h = 0.5$.

these effects, however, do not manifest a change in convergence rates with the increase in ν (all curves in Fig. 8 are still parallel to each other) and therefore do not represent locking.

5.5. Curved elements: hollow sphere under internal pressure

Our next example is a 3D loading case with curved elements, namely, that of a thick-walled hollow sphere under internal pressure, with an exact solution given in Appendix A.5. We set $E = 1000$, $P = 100$, spherical shell radii $r_i = 0.5$, and $r_o = 1$; the domain consists of 24 elements with the radial width $\Delta r = 0.5$. Two orthogonal cross-sections of the sphere and the radial displacement for $\nu = 0.3$ are shown in Fig. 7(b). The same argument about the necessity of initial placement of GLL boundary points onto the surface of the sphere with the machine precision, as in the hollow cylinder case, applies here, otherwise boundary errors will impair an exponential convergence to the analytical solution.

Convergence in the energy norm versus $N^{1/d}$ is shown in Fig. 9 for traction and displacement boundary conditions. Conclusions similar to that of the cylindrical shell domain stay valid, confirming the absence of the effect of problem dimension on the locking properties of the method, as observed with the straight elements.

5.6. Calculation on distorted meshes

To further test the effect of mesh distortion on convergence and locking, we repeat the calculations of Section 5.2 corresponding to a deformation of a unit square under plain strain conditions, on highly-skewed non-orthogonal meshes. The schematic of a skewed mesh configuration as well as that of a base straight element mesh is shown in Fig. 10. We tested two values of the parameter a/L for the skewed mesh configuration: $a/L = 0.1$ and $a/L = 0.01$. These values roughly correspond to the element aspect ratios of 10 and 100, respectively, which represents a very strong value of distortion for quadrilateral elements (Cubit User Documentation, http://cubit.sandia.gov).

Percentage relative error in the energy norm versus $N^{1/d}$ is shown for $a/L = 0.1$ in Fig. 11 for traction and displacement boundary conditions. We see that the general effect of the mesh skewness largely resembles the effect of curvilinear elements:

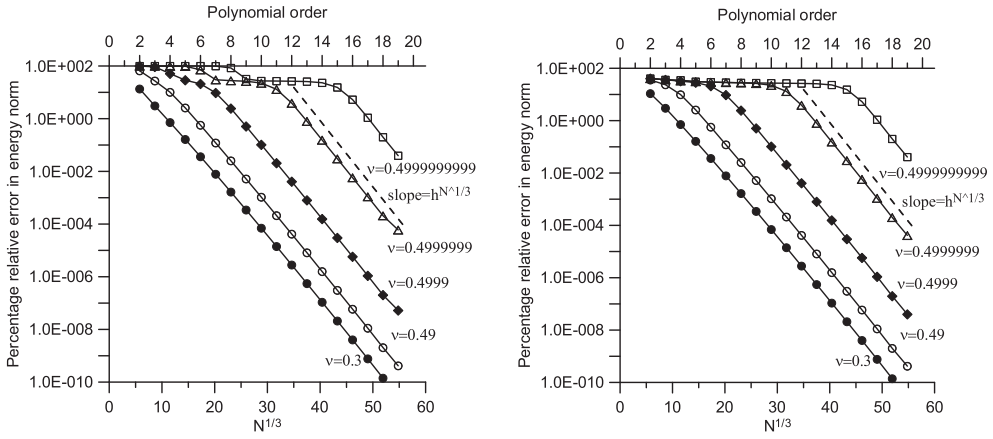

(a) Traction boundary conditions (b) Displacement boundary conditions

Fig. 9. Locking properties for the hollow sphere: error in the energy norm. Dashed line represents the asymptotic curve $h^{N^{1/3}}$, $h = 0.55$.

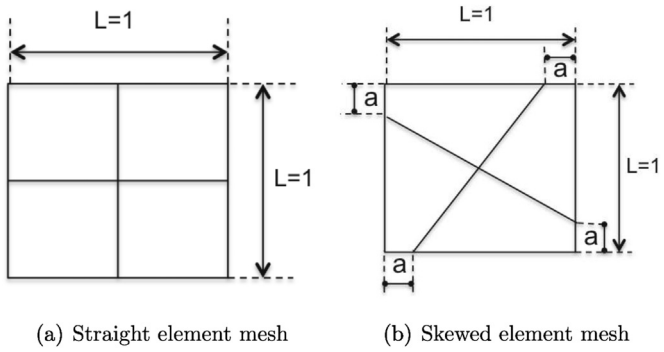

Fig. 10. Schematic of the meshes tested.

convergence for all Poisson ratios slows down (represented by the change of slope in convergence curves from $h = 0.15$ for straight elements to $h = 0.2$ for distorted elements); however, exponential convergence is retained for all Poisson ratios still showing no locking, albeit that, as with curvilinear elements, the onset of convergence is delayed to higher polynomial orders for large values of the Poisson ratios. The comparison of performance of the two distorted meshes of different aspect ratios with that of a straight mesh is shown in Fig. 12. The conclusions stated above remain valid; highly-distorted mesh with a very large aspect ratio of 100 behaves quite poorly in a nearly incompressible situation of $\nu = 0.4999999999$ showing a significant delay in the onset of convergence with the polynomial order.

5.7. Order of locking

In the current section, we summarize the order of robustness deduced from the error plots in all the cases and calculate the order of locking from the order of robustness. Results are printed in Table 1. Order of locking for all the test cases is zero.

6. Computational effort

Incompressibility condition of $\nu \to 0.5$ can not only influence the solution accuracy and the rate of error decay but also the computational efficiency due to the fact that the condition number of the

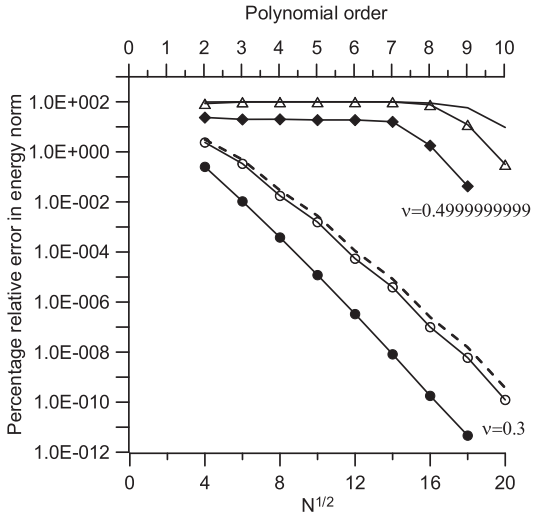

Fig. 12. Comparison between the distorted meshes and a straight mesh for the Poisson ratios of $\nu = 0.3$ and $\nu = 0.4999999999$. Filled symbols, straight mesh; hollow symbols, distorted mesh with $a/L = 0.1$; no symbols, distorted mesh with $a/L = 0.01$.

stiffness matrix grows with the polynomial order and with the Poisson's ratio (Pavarino and Widlund, 2000a). As a consequence, iterative solution of the linear system (19) can take increasingly large number of iterations to converge. To investigate the influence of the Poisson's ratio on the convergence of the conjugate gradient method (CG), we plot the number of iterations of the CG method versus the polynomial degree for several test problems: for square and cube in Fig. 13, and for cylinder and sphere in Fig. 14. Following a study of Pavarino (1997) for mixed spectral element methods, we take the initial guess to be zero and the stopping criterion to be $\|r_i\|_{L_2}/\|r_0\|_{L_2} < 10^{-6}$, where r_i is the ith residual. Figures on the left represent the case when no preconditioning is employed, and figures on the right use a simple preconditioner (inexact mass-matrix preconditioner) equal to the numerical value of the mass matrix obtained by discretizing the term $\int_\Omega \mathbf{u}\cdot\mathbf{v}d\Omega$ on GLL grid. Note that no attempt to optimize the choice of a preconditioner was made in the current study. It is seen that even this simple preconditioner works very well for the problems with curved elements (cylinder and sphere) reducing the number of iterations by about two orders

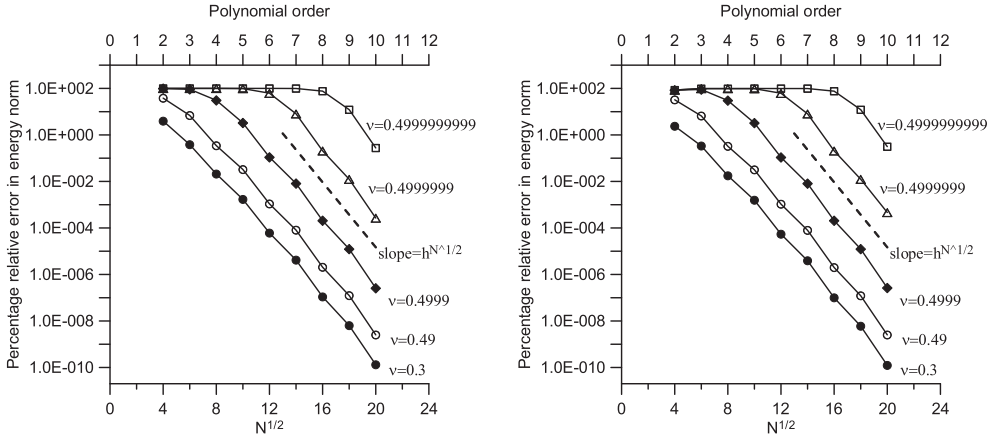

Fig. 11. Locking properties for the unit square on a distorted mesh with $a/L = 0.1$: error in the energy norm. Dashed line represents the asymptotic curve $h^{N^{1/2}}$, $h = 0.2$.

Table 1
Order of robustness and order of locking for the calculated test cases.

	Best approximation rate	Order of robustness	Order of locking, r
	$F_0(N)$	$g(N)$	$f(N) = O(N^r)$
2D, straight elements	$0.15^{N^{1/2}}$	$0.15^{N^{1/2}}$	0
2D, skewed elements	$0.2^{N^{1/2}}$	$0.2^{N^{1/2}}$	0
3D, straight elements	$0.15^{N^{1/3}}$	$0.15^{N^{1/3}}$	0
2D, curved elements	$0.5^{N^{1/2}}$	$0.5^{N^{1/2}}$	0
3D, curved elements	$0.55^{N^{1/3}}$	$0.55^{N^{1/3}}$	0

of magnitude in some cases. This preconditioner, however, does not seem to be effective for the problems with straight elements (square and cube). As can be judged from the log–log plots, the number of iterations of the preconditioned method grows as a power of the polynomial degree p (with linear growth in most cases), comparable to the results of Pavarino for mixed methods (Pavarino, 1997). Unlike in the study of Pavarino (1997), the dependence on the Poisson's ratio shows non-monotonic behavior.

To compare the efficiency of the present displacement-based algorithm with that of mixed methods, we compare the number of iterations taken by our method with the number of iterations in $Q_n - P_{n-1}$ mixed spectral-element method in the study of Pavarino (1997). To maximize the match of the computational conditions, we report results obtained on a cube $[-1,1]^3$ and compare them to the results of Pavarino (1997) obtained on a cube $[-1,1]^3$, one element is used in both studies. Unfortunately, exact match of the computational conditions is not possible, since, as mentioned before, Conjugate Gradient method is not applicable to a symmetric indefinite system of a mixed formulation that was solved with the closely related Conjugate Residual method by Pavarino (1997). In addition, preconditioners were different: inexact mass-matrix preconditioner in this study, and inexact stiffness-matrix preconditioner in Pavarino (1997).

Results for this comparison are presented in Table 2. We put the data obtained with $\nu = 0.4999999999$ in the column with $\nu = 0.5$, since the exact value of $\nu = 0.5$ would make the system singular in our method. The table shows that the displacement method with its particular combination of iterative solver/preconditioner is slightly more efficient at low polynomial orders than the mixed method with its particular combination of iterative solver/preconditioner, as described above, but becomes less efficient at large polynomial orders and Poisson's ratios in the range of 0.499–0.49999. The recovery of the current method for $\nu > 0.49999$ is an interesting attribute and deserves further investigation in the future.

We admit that comparing these two methods with different iterative solvers and preconditioners does not allow us to make definite conclusions about the superiority of one method versus another in terms of computational efficiency. Rather, it tells us that both methods, in their unoptimized form, show roughly similar iteration counts and don't differ by orders of magnitudes in efficiency. We also acknowledge that there is a potential for both methods to improve in efficiency. Indeed, inexact preconditioner in the study of Pavarino (1997) is the worst-case scenario: better

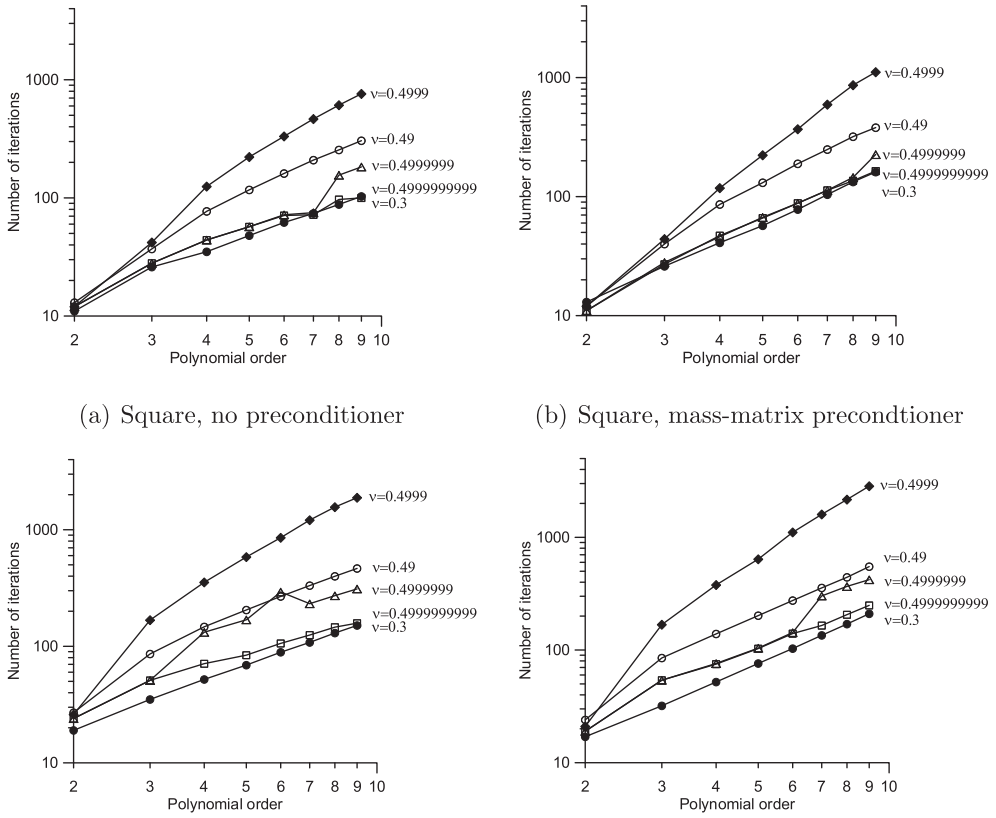

(a) Square, no preconditioner (b) Square, mass-matrix precondtioner

(c) Cube, no preconditioner (d) Cube, mass-matrix preconditioner

Fig. 13. Number of iterations of the conjugate gradient method for the square (4 elements) and the cube (8 elements). Top figures correspond to the square; bottom, to the cube. Left figures correspond to CG without preconditioner; right, with preconditioner.

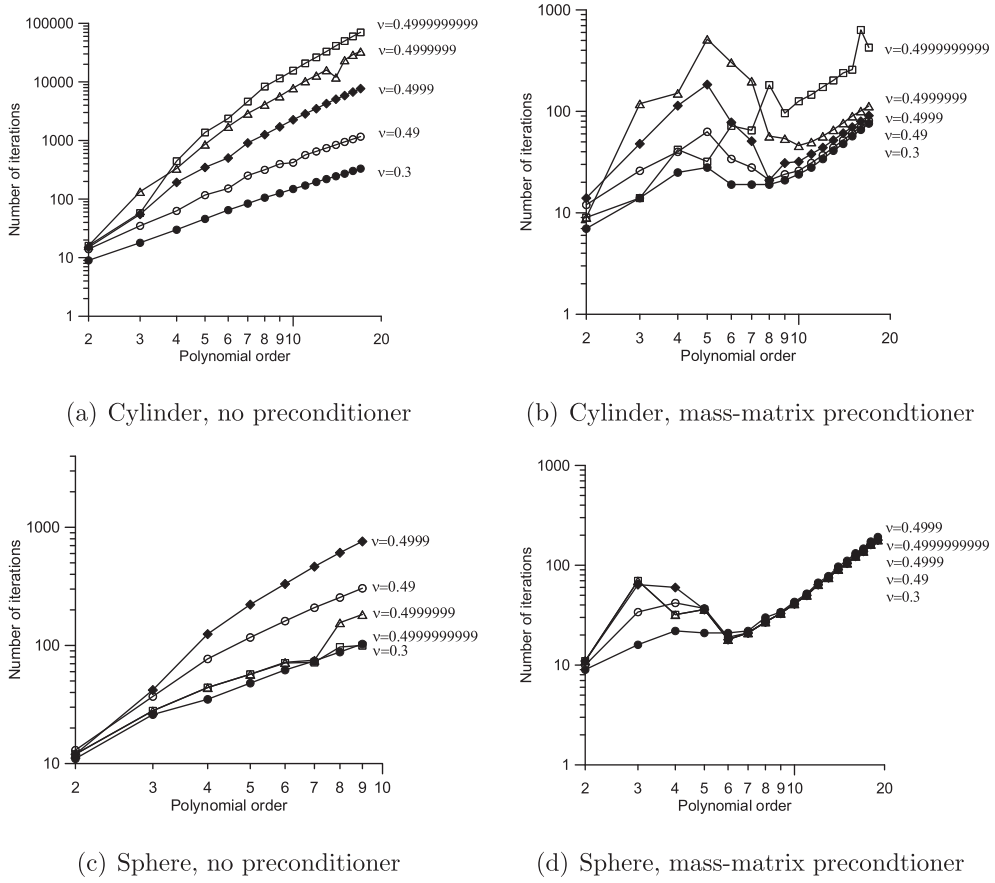

Fig. 14. Number of iterations of the conjugate gradient method for the cylinder (6 elements) and the sphere (24 elements). Top figures correspond to the cylinder; bottom, to the sphere. Left figures correspond to CG without preconditioner; right, with preconditioner.

iteration counts are obtained when exact block-diagonal preconditioner is used. The preconditioner used in the current study has not been optimized, and likely better efficiency can be obtained in the current method as well once this is done. We note that studies addressing the choice of a good preconditioner for the current method and comparing results with mixed methods with a better match of the computational conditions would be beneficial and will be performed in the future.

Table 2
Comparison of the number of iterations between the displacement (direct) and the mixed $Q_n - P_{n-1}$ (Pavarino, 1997) spectral element methods.

p	ν	0.3	0.4	0.49	0.499	0.4999	0.49999	0.499999	0.5
3	Direct	2	2	2	2	2	2	2	2
	Mixed	14	14	14	14	14	14	14	14
4	Direct	7	7	8	8	8	8	8	8
	Mixed	27	30	36	37	37	37	37	37
5	Direct	13	15	16	17	15	14	12	12
	Mixed	34	40	56	61	61	61	61	61
6	Direct	18	21	36	41	39	35	22	22
	Mixed	42	49	68	75	75	75	75	75
7	Direct	22	27	45	48	48	41	23	23
	Mixed	46	54	80	87	87	87	87	87
8	Direct	27	33	67	99	107	95	61	36
	Mixed	52	61	92	102	103	103	103	104
9	Direct	32	39	77	97	121	78	53	33
	Mixed	55	65	97	109	109	109	109	109
10	Direct	37	46	97	163	201	150	86	49
	Mixed	57	69	107	121	121	121	122	122

7. Conclusions

In this paper, we investigate convergence properties of the Legendre spectral element approximation with displacement formulation of linear elasticity equations for a range of Poisson's ratios from a compressible regime ($\nu = 0.3$) to nearly incompressible regime ($\nu = 0.4999999999$). Several numerical examples are considered, including problems with straight elements in 2D and 3D as well as problems with curved elements in 2D and 3D and on distorted meshes. Following the mathematical definition of locking (Babuška and Suri, 1992a, 1992b; Suri, 1996), we calculate a computable measure of locking, the order of robustness. The order of locking calculated from the order of robustness is zero for all the cases. This shows the absence of Poisson locking in the energy norm for displacement-based spectral-element discretization of linear elasticity equations, consistent with previous observations with p and hp finite elements. Although the procedure is free from locking in the asymptotic sense, the polynomial order at which convergence starts increases as the Poisson's ratio gets close to 0.5, and it further increases when the curved elements or highly-distorted meshes are used. Preliminary comparison of computational efficiency of the current method with $Q_n - P_{n-1}$ mixed spectral-element method of Pavarino (1997) shows similar iteration counts of the iterative solver. Future studies will address comparing different preconditioning techniques for the current method and choosing an optimum preconditioner, as well as performing comparison with other methods at a closer match of computational conditions.

Acknowledgments

This work has been initiated when Y.P. was an NSF RTG post-doctoral fellow at the Department of Engineering Sciences and Applied Mathematics at Northwestern University. We acknowledge the financial support of the NSF RTG grant DMS-0636574 at Northwestern University and the SHARP project of the U.S. Department of Energy, under Contract DE-AC02-06CH11357.

Appendix A. Exact Solutions to the Test Problems

Appendix A.1. Bending of a narrow cantilever beam

For the bending of a narrow cantilever beam with rectangular cross-section of length L and height d, under the end load P applied at $x = 0$ and fixed at the point $x = L$, $y = 0$, the following exact solution exists for the horizontal displacement u and the vertical displacement v (Wang, 1953):

$$u = -\frac{P}{2EI}x^2y + \frac{P}{3EI}\left(1+\frac{\nu}{2}\right)y^3 + \frac{P}{2EI}\left[L^2 - (1+\nu)\frac{d^2}{2}\right]y,$$
$$v = \frac{\nu P}{2EI}xy^2 + \frac{P}{6EI}x^3 - \frac{PL^2}{2EI}x + \frac{PL^3}{3EI}.$$

Here $I = d^3/12$ is the cross-sectional moment of inertia.

Appendix A.2. Deformation of a unit square

For a unit square $[0,1] \times [0,1]$ in plane strain conditions under forcing

$$f_x = A_x\sin(ax)\cos(by),$$
$$f_y = A_y\cos(ax)\sin(by),$$

where

$$A_x = (Aa^2 + Bab)(\lambda+\mu) + A(a^2+b^2)\mu,$$
$$A_y = (Bb^2 + Aab)(\lambda+\mu) + B(a^2+b^2)\mu,$$

the following exact solutions exist:

$$u = A\sin(ax)\cos(by),$$
$$v = B\cos(ax)\sin(by).$$

Appendix A.3. Deformation of a unit cube

For a unit cube $[0,1] \times [0,1] \times [0,1]$ under forcing

$$f_x = A_x\sin(ax)\cos(by)\cos(cz),$$
$$f_y = A_y\cos(ax)\sin(by)\cos(cz),$$
$$f_z = A_z\cos(ax)\cos(by)\sin(cz),$$

where

$$A_x = (Aa^2 + Bab + Cac)(\lambda+\mu) + A(a^2+b^2+c^2)\mu,$$
$$A_y = (Bb^2 + Aab + Cbc)(\lambda+\mu) + B(a^2+b^2+c^2)\mu,$$
$$A_z = (Cc^2 + Aac + Bbc)(\lambda+\mu) + C(a^2+b^2+c^2)\mu,$$

the solutions are

$$u = A\sin(ax)\cos(by)\cos(cz),$$
$$v = B\cos(ax)\sin(by)\cos(cz),$$
$$w = C\cos(ax)\cos(by)\sin(cz).$$

Appendix A.4. Hollow cylinder under internal pressure

For a plane strain hollow cylinder with the inner radius r_i and the outer radius r_o under internal pressure P and zero external pressure (satisfying boundary conditions $\sigma_r(r_i) = -P, \sigma_r(r_o) = 0$), the displacements in cylindrical coordinates have the form (Gao, 2003)

$$u_r = \frac{1+\nu}{E}\frac{Pr_i^2}{r_o^2 - r_i^2}\left[(1-2\nu)r + \frac{r_o^2}{r}\right],$$
$$u_\theta = 0, u_z = 0.$$

Appendix A.5. Hollow sphere under internal pressure

For a hollow sphere with the inner radius r_i and the outer radius r_o under internal pressure P and zero external pressure (satisfying boundary conditions $\sigma_r(r_i) = -P, \sigma_r(r_o) = 0$), the displacements in spherical coordinates have the form (see (Fung, 1965))

$$u_r = \frac{1}{E}\frac{Pr_i^3}{r_o^3 - r_i^3}\left[(1-2\nu)r + (1+\nu)\frac{r_o^3}{2r^2}\right],$$
$$u_\theta = 0, u_\phi = 0.$$

References

Babuška, I., Suri, M., 1990. The p and $h-p$ versions of the finite element method, an overview. Comp. Meth. Appl. Mech. Eng. 100, 249–273.
Babuška, I., Suri, M., 1992. Locking effects in the finite element approximation of elasticity problems. Numer. Math. 62, 439–463.
Babuška, I., Suri, M., 1992. On the locking and robustness in the finite element method. SIAM J. Numer. Anal. 29, 1261–1293.
Babuška, I., Suri, M., 1994. The p and $h-p$ versions of the finite element method, basic principles and properties. SIAM Rev. 36, 578–632.
Bathe, K.J., 1996. Finite Element Procedures. Prentice Hall.
Brezzi, F., Fortin, M., 1991. Mixed and Hybrid Finite Element Methods. Springer, Berlin.
Brigham, J.C., Aquino, W., Aguilo, M.A., Diamessis, P.J., 2011. A spectral finite element approach to modeling soft solids excited with high-frequency harmonic loads. Comp. Meth. Appl. Mech. Eng. 200, 692–698.
Brito, K.D., Sprague, M.A., 2012. Reissner-Mindlin Legendre spectral finite elements with mixed reduced quadrature. Fin. El. Anal. Des. 58, 74–83.
Casadei, F., Geabellini, E., Fotia, G., Maggio, F., Quarteroni, A., 2002. A mortar spectral/finite element method for complex 2D and 3D elastodynamics problems. Comp. Meth. Appl. Mech. Eng. 191, 5119–5148.
Chaljub, E., Capdeville, Y., Vilotte, J.-P., 2003. Solving elastodynamics in a fluid-solid heterogeneous sphere: a parallel spectral element approximation on non-conforming grids. J. Comp. Phys. 187, 457–491.
Chapelle, D., Bathe, K.J., 1993. The inf-sup test. Comput. Struct. 47, 537–545.
Chilton, L., Suri, M., 1997. On the selection of a locking-free hp element for elasticity problems. Int. J. Numer. Meth. Eng. 40, 2045–2062.
Cristini, P., Komatitsch, D., 2012. Some illustrative examples of the use of the spectral-element method in ocean acoustics. J. Acoustic. Soc. Am. 131 (3), EL229–EL235.
Deville, M.O., Fischer, P.F., Mund, E.H., 2002. High-order Methods for Incompressible Fluid Flow. Cambridge University Press, Cambridge, UK.
Dong, S., Yosibash, Z., 2009. A parallel spectral element method for dynamic three-dimensional nonlinear elasticity problems. Comput. Struct. 87, 59–72.
Figueroa, C.A., Vignon-Clementel, I.E., Jansen, K.E., Hughes, T.J.R., Taylor, C.A., 2006. A coupled momentum method for modeling blood flow in three-dimensional deformable arteries. Comput. Methods Appl. Mech. Eng. 195, 5685–5706.
Fischer, P.F., 1997. An overlapping Schwarz method for spectral element solution of the incompressible Navier–Stokes equations. J. Comp. Phys. 133, 84–101.
Fischer, P.F., Patera, A.T., 1991. Parallel spectral element solution of the Stokes problem. J. Comp. Phys. 92, 380–421.
Fung, Y.C., 1965. Foundations of Solid Mechanics. Prentice Hall, Englewood Cliffs, N.J.

Gao, X.-L., 2003. Elasto-plastic analysis of an internally pressurized thick-walled cylinder using a strain gradient plasticity theory. Int. J. Sol. Struct. 40, 6445–6455.
Gopalakrishnan, S., 2002. Behavior of isoparametric quadrilateral family of Lagrangian fluid elements. Int. J. Numer. Meth. Eng. 54, 731–761.
Ha, S., Chang, F.-K., 2010. Optimizing a spectral element for modeling PZT-induced Lamb wave propagation in thin plates. Smart Mater. Struct. 19.
Heisserer, U., Hartmann, S., Duster, A., Yosibash, Z., 2008. On volumetric locking-free behavior of *p*-version finite elements under finite deformations. Comm. Numer. Meth. Eng. 24, 1019–1032.
Hughes, T.J.R., 1987. The Finite Element Method. Prentice Hall.
Humphrey, J.D., 2003. Review paper: continuum biomechanics of soft biological tissues. Proc. R. Soc. Lond. A 459, 3–46.
Jensen, S., Vogelius, M., 1990. Divergence stability in connection with the p-version of the finite element method. Math. Mod. Num. Anal. 25, 737–764.
Karniadakis, G.E., Sherwin, S.J., 2005. Spectral/hp Element Methods for Computational Fluid Dynamics, second ed. Oxford University Press, New York.
Komatitsch, D., Vilotte, J.-P., Vai, R., Castillo-Covarrubias, J.M., Sánchez-Sesma, F.J., 1999. The spectral-element method for elastic wave equations – application to 2D and 3D seismic problems. Int. J. Numer. Meth. Eng. 45, 1139–1164.
Komatitsch, D., Tsuboi, S., Tromp, J., 2005. The spectral-element method in seismology. Geophys. Monogr. 57, 205–227.
Maday, Y., Patera, A., Rønquist, E., 1992. The $P_n \times P_{n-2}$ Method for the Approximation of the Stokes Problem. Tech. Rep. 92009. Dept. of Mech. Engr., MIT.
Malkus, D.S., Hughes, T.J.R., 1978. Mixed finite element mehtods – reduced and selective integration techniques: a unification of concepts. Comp. Meth. Appl. Mech. Eng. 12, 67–76.
Mott, P.H., Dorgan, J.R., Roland, C.M., 2008. The bulk modulus and Poisson's ratio of "incompressible" materials. J. Sound Vibr. 312, 572–575.
Nagtegaal, J.C., Parks, D.M., Rice, J.R., 1974. On numerically accurate finite element solutions in the fully plastic range. Comp. Meth. Appl. Mech. Eng. 4, 153–177.
Orszag, S.A., 1980. Spectral methods for problems in complex geometries. J. Comput. Phys. 37, 70–92.
Patera, A.T., 1984. A spectral element method for fluid dynamics: laminar flow in a channel expansion. J. Comp. Phys. 54, 468–488.
Pavarino, L.F., 1997. Preconditioned mixed spectral element methods for elasticity and Stokes problems. SIAM J. Sci. Comp. 19, 375–402.
Pavarino, L.F., Widlund, O.B., 2000. Iterative substructuring methods for spectral element discretizaion of elliptic systems, I: compressible linear elasticity. SIAM J. Numer. Anal. 37 (2), 375–402.
Pavarino, L.F., Widlund, O.B., 2000. Iterative substructuring methods for spectral element discretizaion of elliptic systems, II: mixed methods for linear elasticity and Stokes flow. SIAM J. Numer. Anal. 37 (2), 353–374.
Pavarino, L.F., Widlund, O.B., Zampini, S., 2010. BDDC preconditioners for spectral element discretizations of almost incompressible elasticity in three dimensions. SIAM J. Numer. Anal. 32 (6), 3604–3626.
Prathap, G., 1993. The Finite Element Methods in Structural Mechanics. Kluwer Academic Press, Dordrecht.
Saad, Y., 2003. Iterative Methods for Sparse Linear Systems, second ed. SIAM, Philadelphia, PA.
Schneidesch, C., Deville, M., 1993. Chebyshev collocation method and multi-domain decomposition for Navier–Stokes equations in complex curved geometries. J. Comput. Phys. 106, 234–257.
Shim, E.B., Kamm, R.D., 2002. Numerical simulation of steady flow in a compliant tube or channel with tapered wall thickness. J. Fluids Struct. 16, 1009–1027.
Sprague, M.A., Geers, T.L., 2007. Legendre spectral finite elements for structural dynamics analysis. Comm. Numer. Meth. Eng. 00, 1–13.
Stupazzini, M., Zambelli, C., 2005. GeoELSEvp: a spectral element approach for dynamic elasto-viscoplastic problems. Riv. It. Geotec. 4, 71–81.
Suri, M., 1996. Analytical and computational assessment of locking in the *hp* finite element method. Comp. Methods Appl. Mech. Eng. 133, 347–371.
Suri, M., Stenberg, R., 1996. Mixed *hp* finite element methods for problems in elasticity and Stokes flow. Numer. Math. 72, 367–390.
Szabó, B., Babuška, I., 1991. Finite-element Analysis. John Wiley & Sons, New York.
Szabó, B.A., Babuška, I., Chayapathy, B.K., 1989. Stress computations for nearly incompressible materials by the *p*-version of the finite element method. Int. J. Numer. Meth. Eng. 28, 2175–2190.
Tromp, J., Komatitsch, D., Liu, Q., 2008. Spectral-element and adjoint methods in seismology. Comm. Comp. Phys. 3, 1–32.
Valencia, A., Solis, F., 2006. Blood flow dynamics and arterial wall interaction in a saccular aneurysm model of the basilar artery. Comput. Struct. 84, 1326–1337.
Vogelius, M., 1983. An analysis of the p-version of the finite element method for nearly incompressible materials: uniformly valid, optimal error estimates. Numer. Math. 41, 39–53.
Wang, C.-T., 1953. Applied Elasticity. McGraw-Hill, New York.
Yosibash, Z., 1996. Accurate stress extraction for nearly incompressible materials by the displacement formulation of the *p*-version FEM. Comm. Numer. Meth. Eng. 12, 807–826.
Yu, H.S., Houlsby, G.T., Burd, H.J., 1993. A novel isoparametric finite element displacement formulation for axisymmetric analysis of nearly incompressible materials. Int. J. Numer. Meth. Eng. 36, 2454–2472.